Applied Water Science (2023) 13:43
https://doi.org/10.1007/s13201-022-01833-x

ORIGINAL ARTICLE

Electrical properties of hematite and pure sand synthetic homogeneous mixture

Mohamed Mahmoud Gomaa[1]

Received: 27 September 2022 / Accepted: 16 November 2022 / Published online: 30 December 2022

Abstract

Substances' electrical properties react promptly to minor alterations in the specimens (texture). This electrical characteristics response depends on pH and, hence, on the surface charge. In this article, we attempt to keep the synthetic specimens homogeneous. Sand and pure hematite is smashed independently and aggregated (hematite were collected from Eastern Desert, Cairo, Egypt). Electrical parameters were examined at frequencies ranging from 0.1 to 10^5 Hz (dry, 21 °C). The electrical range of the measured data varies considerably depending on the frequency spectrum, specimens' concentration, constitution, and/or arrangement of the components (texture). There are two conduction areas relying on frequency-dependent conductivity (two slopes). Dielectric permittivity increases linearly with concentration. Dielectric permittivity is rapidly decreasing as the spectrum expands. Jonscher's law is applicable to all electrical characteristics. The hematite conductor concentration changes in the synthetic specimens and accordingly the texture of the specimens. The study of these electrical characteristics may assist in the modeling and simulation of rock electrical properties. The relationships between the ore's nature, mineral compositions, and electrical properties are valuable for exploration methods.

Keywords Hematite · Conductivity · Permittivity · Dielectric constant · Electric · Pure sand · Impedance

Introduction

Electrical resistivity and induced polarizability are common rock electrical properties used to locate mineral deposit zones and investigate the thermal and compositional structure of the Earth's core. The exploration and interpretation of the electrical characteristics of conducting and semiconducting components in combinations have recently gained popularity. There are just a few analytical considerations of electrical conductivity in composite materials. As a result, it is critical to identify the analytical display of electrical characteristics of mixtures in proportion to conductor concentration (Capozzoli et al. 2022). It is also necessary to explain the specimen's texture and electrical transfer processes (Lima 1995; Gomaa 2009, 2013).

Low-frequency electrical spectroscopy is very valuable, as it provides more information than static electrical measurements of mobility or conductivity. Experiments have proved that the dielectric response is very sensitive to the conductor properties (as will be seen below). Moreover, the amplitude and the frequency dependence of the response are related to transport processes around the particles or grains, which, in their turn, depend on the double layer structure and the particle or grains' shape. Low-frequency dielectric spectroscopy involves major technical problems related to electrode polarization in combination with unfavorable phase angles of the impedances, and the four-electrode technique may solve this problem. Measurement of the static conductivity does not suffer from such technical problems.

Electrical transport techniques in any composite are primarily determined by the volume ratios of the conductors and insulators, as well as the relationship of each component in the specimen (Gomaa 2008; Olhoeft 1985). The effective electrical characteristics of shaly sands are mostly determined by particle size (Lima and Sharma 1991, 1992). Furthermore, electrical characteristics are affected by particle shape (Sen 1981, 1984, Gomaa and Abou El-Anwar 2017), the effective electrical linkages of creating and occupying interstices (Chew and Sen 1982; Vinegar and Waxman 1984; Sen 1989), random connections, and composite heterogeneity (Abou El-Anwar and Gomaa 2013). Textural

✉ Mohamed Mahmoud Gomaa
mmmsgomaa@yahoo.com

[1] Head of Geophysical Exploration Group, Geophysical Sciences Department, National Research Centre, El-Tahrir St., Dokki 12311, Egypt

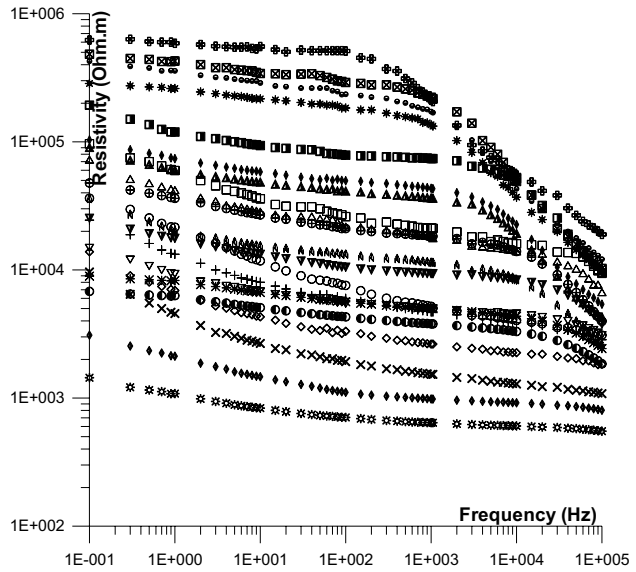

Fig. 1 Electrical performance of resistivity values as a function of frequency for samples with varied sand percentages (☼ 0, ♦ 5, ✕ 10, ◇ 15, ◐ 20, ✳ 25, + 30, ○ 35, ▽ 40, ▼ 45, ⋔ 50, ⊕ 55, △ 60, □ 65, ▲ 70, ♦ 75, ◨ 80, ✷ 85, ● 90, ⊠ 95, and ✙ 100%)

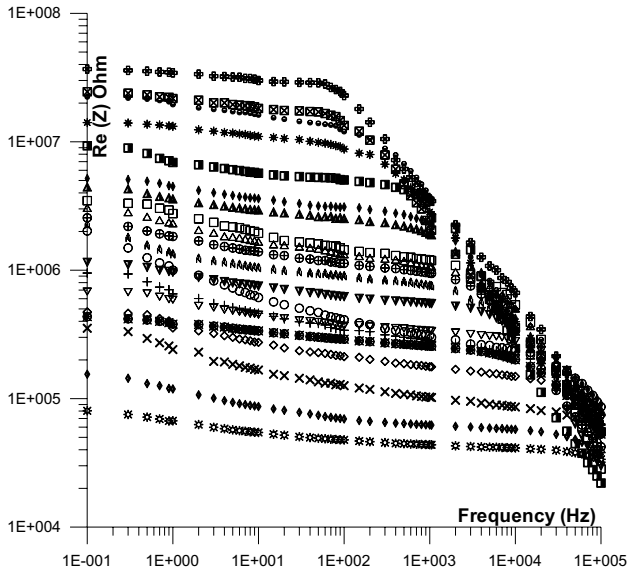

Fig. 3 Electrical performance of real impedance values as a function of frequency for samples with varied sand percentages (☼ 0, ♦ 5, ✕ 10, ◇ 15, ◐ 20, ✳ 25, + 30, ○ 35, ▽ 40, ▼ 45, ⋔ 50, ⊕ 55, △ 60, □ 65, ▲ 70, ♦ 75, ◨ 80, ✷ 85, ● 90, ⊠ 95, and ✙ 100%)

heterogeneities or geometric parameters of specimens change contact electrical characteristics (Sen, 1981; Knight and Endres, 1990; Knight and Nur 1987), or interface reactions (Maxwell–Wagner relaxation process) between grains (Marshall and Madden, 1959; Dias, 1972; Dukhin and Shilov, 1974; Chew and Sen, 1982).

The permittivity (ε) has a power-law dependency relationship with frequency (w) (Franceschetti and Macdonald 1977; Glover et al. 1994; Gomaa et al. 2009; Gomaa et al. 2000; Gomaa 2006, 2022; Huggins 1975; Jonscher 1977; Kassab et al. 2017; Kurien et al. 2006; Levitskaya and Sternberg 2000; Macdonald 1974; Shaltout et al. 2012; Simon and Franke 2000). This association is most likely influenced by the texture of the

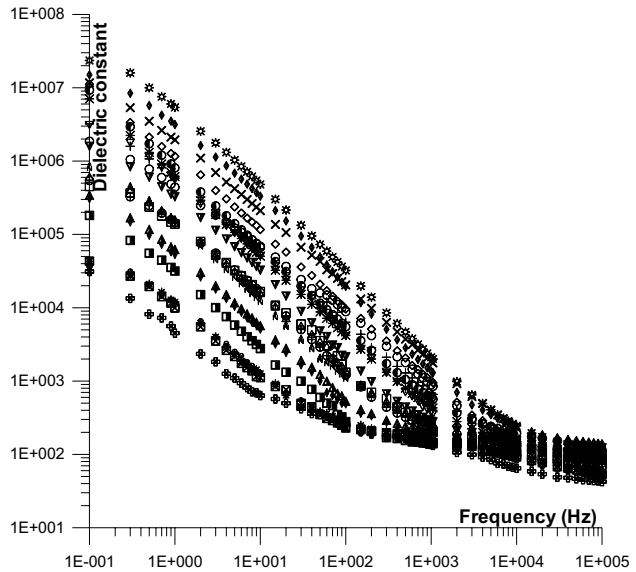

Fig. 2 Electrical performance of dielectric constant values as a function of frequency for samples with varied sand percentages (☼ 0, ♦ 5, ✕ 10, ◇ 15, ◐ 20, ✳ 25, + 30, ○ 35, ▽ 40, ▼ 45, ⋔ 50, ⊕ 55, △ 60, □ 65, ▲ 70, ♦ 75, ◨ 80, ✷ 85, ● 90, ⊠ 95, and ✙ 100%)

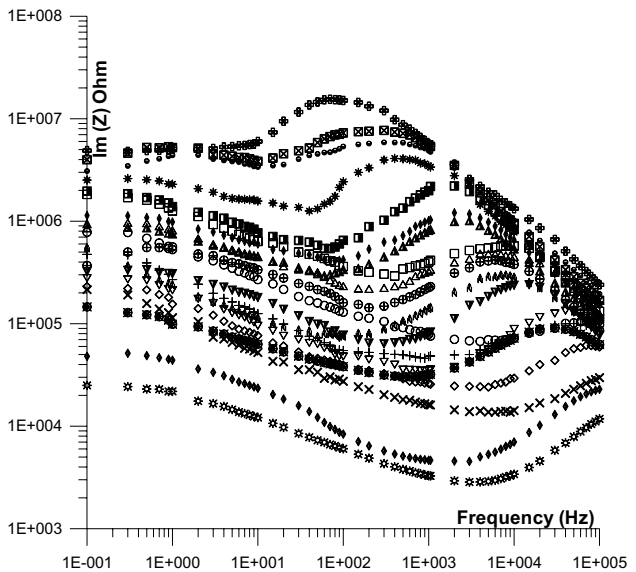

Fig. 4 Electrical performance of imaginary impedance values as a function of frequency for samples with varied sand percentages (☼ 0, ♦ 5, ✕ 10, ◇ 15, ◐ 20, ✳ 25, + 30, ○ 35, ▽ 40, ▼ 45, ⋔ 50, ⊕ 55, △ 60, □ 65, ▲ 70, ♦ 75, ◨ 80, ♦ 85, ✕ 90, ⊠ 95, and ✙ 100%)

specimens (Knight and Abad 1995; Knight 1983). Furthermore, the random connections of the grains inside the specimens may be the primary cause of the power-law response (Jonscher 1999, Gomaa et. al. 2000, 2018). The interface between grains will cause considerable frequency dependency with a high permittivity value for a combination of semiconductor and insulator (pure hematite and pure sand mixture) (Chelidze et al. 1999; Gomaa 2022). This is explained by the polarization mechanism or surface conductivity responses.

The presence of an insulator grain covered with a semiconducting one and surrounded by an alternating current field causes high permittivity values, particularly at low frequencies (Chelidze and Gueguen 1999). As a result, the addition of a tiny conductor (or semiconductor) to an insulator component causes high permittivity values to be initiated at a low frequency. In addition, the presence of insulator particles between the conducting particles and/or covering them may reduce conductivity. As a result, there may be a notable rise in the dielectric constant, particularly at low frequencies (Gomaa and Alikaj 2009; Gomaa and Elsayed 2009).

The electrical response of twenty-two homogeneous composites of hematite and pure sand samples (Eastern Desert, Cairo, Egypt) with varying hematite concentrations is of interest in the following paragraphs. Electrical characteristics were measured at a dry state with frequencies ranging from 0.1 to 10^5 Hz (dry, 21 °C). These samples ensure that the specimens are uniformly homogeneous and tidily oriented. Specimens were ground, flipped over, and ultimately compacted. The physical theories and mechanisms of conduction and polarization that may result from varying the concentrations of mixture components will be explored. The uniqueness of the study stems from the removal of the textural impact of the samples, with the sole variable in the samples being the change in conductor concentration.

Hematite general properties

Hematite is a dense and hard mineral that is the most significant iron ore due to its high iron concentration and abundance (Gomaa et al. 2015). The mineral may be found in a variety of forms, including steel-gray crystals and coarse-grained variants (Gomaa and Alikaj 2009). It can also be found as short, black rhombohedra crystals with an iridescent tarnish. Hematite pigment is a soft, fine-grained, earthy type of hematite. Hematite deposits of significant size can be found in sedimentary beds or metamorphosed sediments. It comes in black, silver-gray, brown, reddish-brown, and red. Although brittle, it is harder than pure iron (Nakhla and Shehata 1967).

Hematite (α-Fe_2O_3) is one of four forms of iron oxides: wustite ($Fe_{1-x}O$), magnetite (Fe_3O_4), maghemite (γ-Fe_2O_3). They are based on a closely packed O^{2-} anion lattice, with the smaller Fe cations occupying octahedrally and tetrahedrally coordinated interstices in between. α-Fe_2O_3 are within Fe^{2+} in octahedral sites. Hematite can be obtained from goethite (Nakhla and Shehata 1967).

Hematite rock may be found in several geologic formations in nature (igneous, metamorphic and sedimentary). Iron ores, futile, tourmaline, and zircon are the most prevalent heavy minerals detected in hematite samples (Attia 1955). Conglomerates, sandstones, sand and shales, clay, and quartz make up the iron-ore layers. It is frequently found in association with ferruginous sandstones and particular clay minerals, and there are multiple transitions from ferruginous sandstone to oolitic iron-ore (Shukri and Ayouty, 1959). Ferruginous sandstones may contain iron ore-containing oolites mineralogically (Nakhla and Shehata 1967). Furthermore, a small percentage of quartz grains may include modest hematite impurities. Some strata of ferruginous sandstones include sub-angular debris grains. It is the consequence of quartz and hematite intergrowth or hematite, goethite, and quartz intergrowth (goethite is partially replacing hematite). The iron ore in Eastern Desert, Cairo, Egypt, is Crypto-crystalline hydrated hematite (Fe_2O_3-nH_2O). There may be some microcrystalline hematite grains in addition to clay particles. Amorphous and cryptocrystalline pure sand, as well as quartz grains and other components, may be present in some samples (goethite and hydro goethite). The oolites are composed of two parts: an iron component and quartz, colloidal pure sand, and ferruginous clay (Gason et al. 1999). The elements that may be found in the iron-ore samples, according to the spectrographic inspection, include Cu, Ni, Co, Ti Cr, V, Zr, and Pb. Iron, pure sand, and calcium may be present in the eastern desert, iron-ore deposits as carbonate or sulfate staining or as components of some clay minerals. Other minor components include magnesium, manganese, calcium phosphate, calcium sulfate, copper, titanium, nickel, chromium, and zirconium (Taylor and Ahrens 1960).

Experimental electrical methods

The electrical properties of twenty-two homogeneous composites of pure sand and hematite samples (Eastern Desert, Cairo, Egypt) with various hematite concentrations were investigated. A Hioki 3522–50 LCR Hitester Impedance Analyzer was used to measure complex impedance in a dry condition at constant temperature (~21 °C) throughout

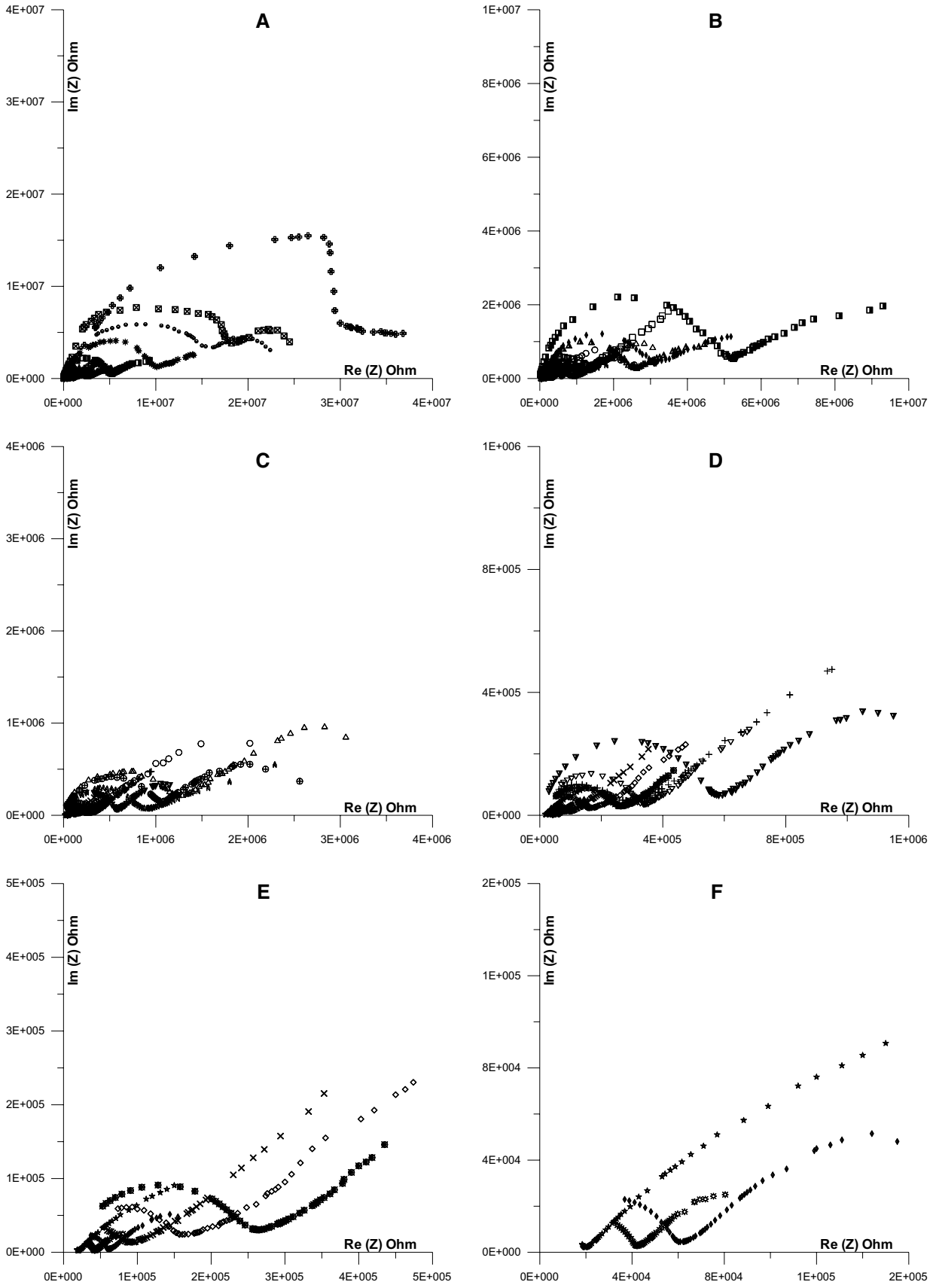
A
Im (Z) Ohm
Re (Z) Ohm
4E+007
3E+007
2E+007
1E+007
0E+000
0E+000
1E+007
2E+007
3E+007
4E+007
B
Im (Z) Ohm
Re (Z) Ohm
1E+007
8E+006
6E+006
4E+006
2E+006
0E+000
0E+000
2E+006
4E+006
6E+006
8E+006
1E+007
C
Im (Z) Ohm
Re (Z) Ohm
4E+006
3E+006
2E+006
1E+006
0E+000
0E+000
1E+006
2E+006
3E+006
4E+006
D
Im (Z) Ohm
Re (Z) Ohm
1E+006
8E+005
4E+005
0E+000
0E+000
4E+005
8E+005
1E+006
E
Im (Z) Ohm
Re (Z) Ohm
5E+005
4E+005
3E+005
2E+005
1E+005
0E+000
0E+000
1E+005
2E+005
3E+005
4E+005
5E+005
F
Im (Z) Ohm
Re (Z) Ohm
2E+005
1E+005
8E+004
4E+004
0E+000
0E+000
4E+004
8E+004
1E+005
2E+005

◂**Fig. 5** Electrical performance of real and imaginary impedance values as a function of frequency for samples with varied sand percentages (0, 5, 10, 15, 20, 25, 30, 35, 40, 45, 50, 55, 60, 65, 70, 75, 80, 85, 90, 95, and 100%)

a frequency range of 0.1–10^5 Hz. Specimens were measured in relative humidity (~55% RH) in an isolated room (dissector).

Specimens were grounded and we used compression of 140 KN to compact the samples into discs. The particle size was ~1 µm. The specimens were then electrically measured after these steps and they had a thickness of ~3 mm and a diameter of 16 mm (the effect of thickness and diameter were removed from the measurements). The dimension of the samples was taken at 1:5 (thickness to diameter) to remove most of the errors to the edge effect. A voltage of around 1 V was applied to the specimens.

The measured electrical properties of the mixture were made in the parallel mode. The measured parameters were the parallel conductance (G_p) and capacitance (C_p) at various frequencies. Complex permittivity can be written as $\varepsilon * = \varepsilon' - i\varepsilon''$, where the real part of the complex dielectric constant $\varepsilon' = C_p d/\varepsilon_0 A$ and the imaginary part $\varepsilon'' = G_p d/w\varepsilon_0 A$, where A is the cross-sectional area of the specimen, d is the thickness of the specimen, ε_0 is permittivity for free space (8.85×10^{-12} F/m), and w is the angular frequency. The dielectric constant and conductivity are calculated from the following equations, $\sigma = dG_p/A$, $\varepsilon' = C_p/C_0$, $C_o = (A/d)\varepsilon_0$. The error of the measurement was in the order of ±5%.

Results and discussion

In general, a rise in the number of homogeneous conducting components (hematite) results in a change in electrical properties (dielectric constant and conductivity). The insertion of conduction connections increases conductivity and the conduction processes. Furthermore, when the hollow volumes between soil conducting grains diminish, so does the permittivity. Many variables, such as frequency, pressure, chemical reaction, and many more, may induce or enable comparable electrical qualities (Gomaa and Kassab 2016, 2017, Gomaa et al. 2015).

Hematite and pure sand are the primary constituents of specimens. Hematite is believed to be a semiconductor, whereas pure sand is assumed to be an insulator (Chirita and Grozescu 2009). As may be seen from the measured electrical conductivity values, the conductivity of specimens ranges from insulator (for reasonably pure sand) to semiconductor (for high concentrations of semiconductor or hematite).

Figure 1 depicts the electrical performance of resistivity values as a function of frequency for samples with varied pure sand percentages (0, 5, 10, 15, 20, 25, 30, 40, 50, 55, 35, 80, 60, 70, 75, 95, 65, 85, 90, and 100 percent). The

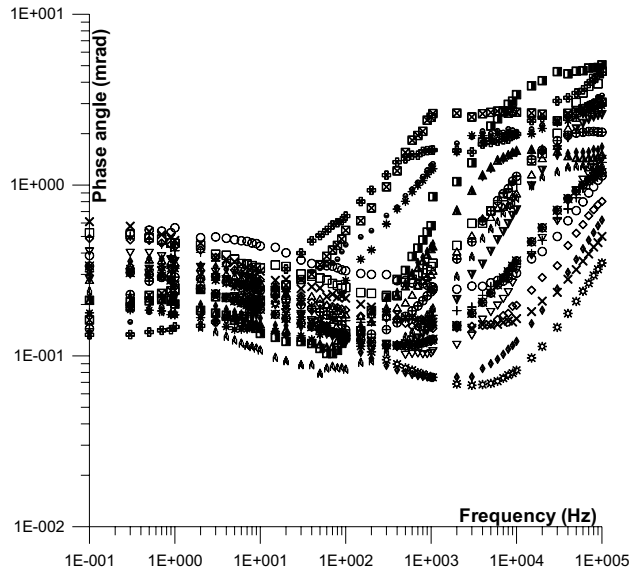

Fig. 6 Electrical performance of phase angle values as a function of frequency for samples with varied sand percentages (0, 5, 10, 15, 20, 25, 30, 35, 40, 45, 50, 55, 60, 65, 70, 75, 80, 85, 90, 95, and 100%)

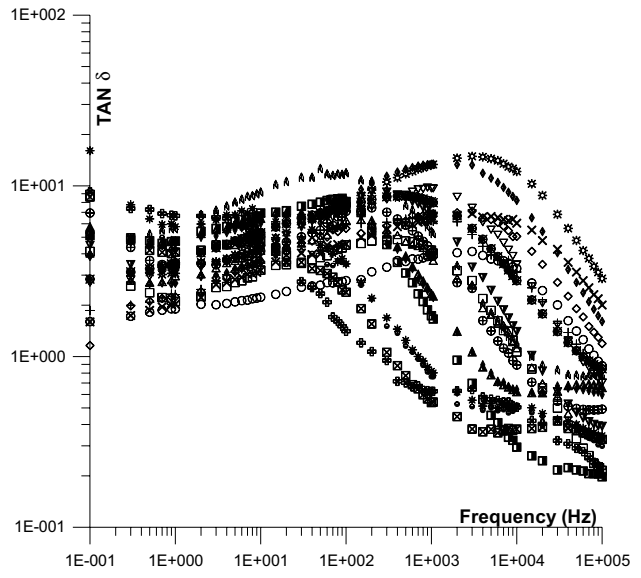

Fig. 7 Electrical performance of dielectric loss (loss tangent, tan δ) values as a function of frequency for samples with varied sand percentages (0, 5, 10, 15, 20, 25, 30, 35, 40, 45, 50, 55, 60, 65, 70, 75, 80, 85, 90, 95, and 100%)

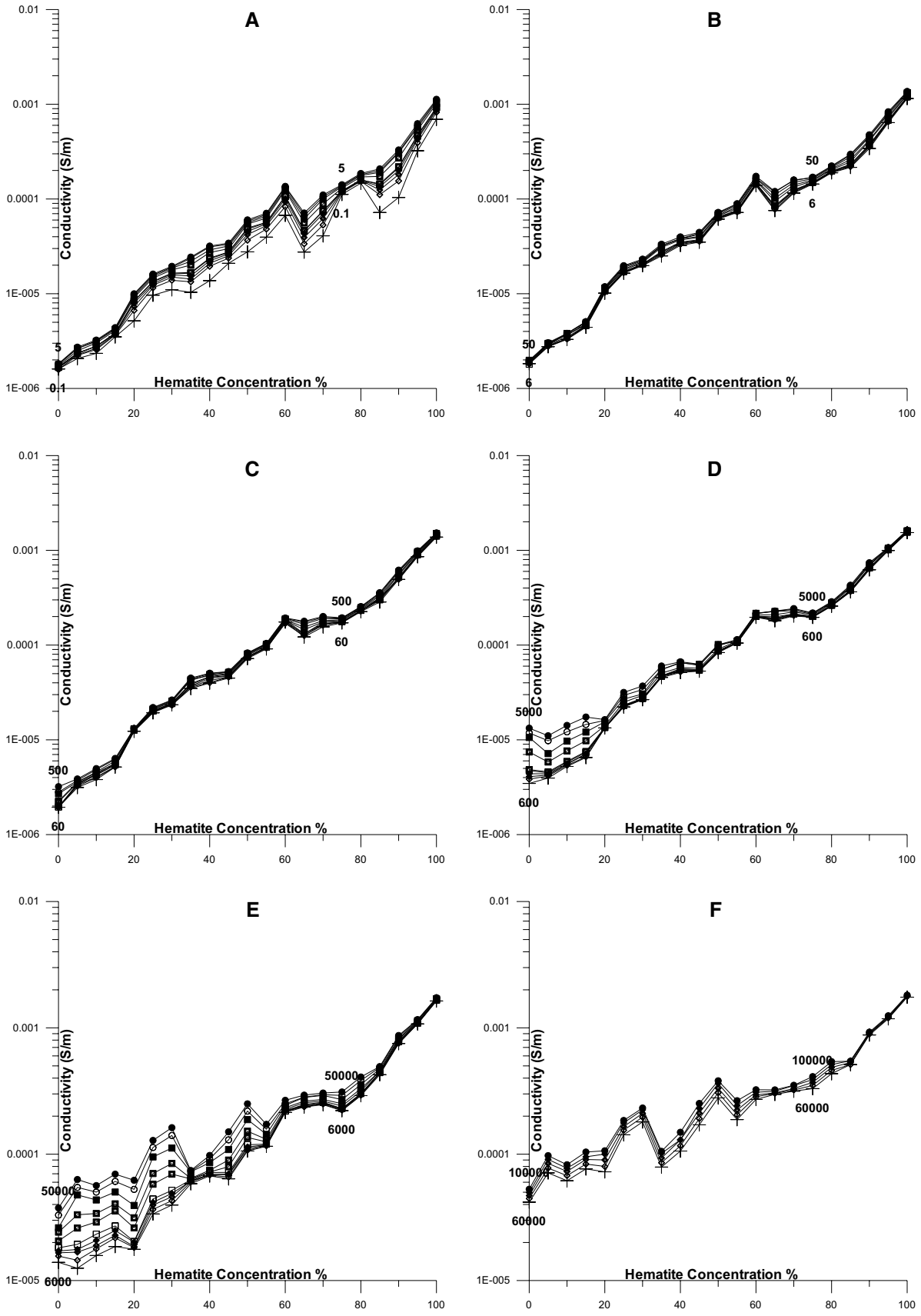
A
B
C
D
E
F
Conductivity (S/m)
Hematite Concentration %
0.01
0.001
0.0001
1E-005
1E-006
0
20
40
60
80
100
5
0.1
50
6
500
60
5000
600
50000
6000
100000
60000

◂**Fig. 8** Electrical performance of conductivity values as a function of hematite concentration percentage for samples with varied frequencies [**A** for 0.1 to 5 Hz; **B** for 6 to 50 Hz; **C** for 60 to 500 Hz; **D** for 600 to 5 kHz; **E** for 6 kHz to 50 kHz; **F** for 60 kHz to 100 kHz].

resistivity values are classified into two groups. The first group has two slopes (due to the high pure sand concentration), whereas the second group has only one (low sand concentration). With low hematite concentrations, the slope of the first category is virtually zero (up to 100 Hz for 100 percent sand concentration and continues to 10 kHz for higher concentrations), whereas the slope of the second is approximately 0.48. As sand concentration increases, the crossover frequency goes to higher frequencies; it begins at 100 Hz for high sand concentration and ends at 10 kHz for rising hematite concentrations. At very high hematite concentrations (at the currently accessible frequency range), there is no crossover frequency; it may exist at higher frequencies. At relatively low frequencies, there is a slight decrease in resistivity with a frequency increase for pure sand samples (zero percent). The fall down of resistivity with frequency is sharper at higher frequencies. The rise in the activation energy of ions, molecules, and electrons at the specimen supports this conclusion. The resistivity of the specimen decreases from ~ $6X10^5$ (Ohm.m) to ~ $1.5X10^3$ (Ohm.m), at 0.1 Hz, with increasing hematite concentration. Also, the two-slope curves become one-slope curves. The addition of hematite concentrations to the sand improves the conductor pathways and therefore the conductivity.

Figure 2 depicts the electrical performance of dielectric constant values as a function of frequency for samples with varied sand percentages (0, 5, 10, 15, 20, 25, 30, 40, 50, 55, 35, 80, 60, 70, 75, 95, 65, 85, 90, and 100 percent). With two slopes, the dielectric constant values are divided into two groups. The first group (with high sand concentration) has the crossover frequency at early low frequencies (> 100 Hz) and a large percentage of sand concentration. The second group, on the other hand, has the crossover frequency at considerably higher frequencies (> 1 kHz) and a low sand concentration percentage. The slope of the first group is almost 0.3 for low hematite concentrations, whereas the slope of the second category is roughly 0.65. As sand concentration grows, so does the crossover frequency; it starts at ~ 100 Hz for high sand concentration and finishes at 10 kHz with high hematite concentrations. The crossover frequency practically vanishes at very high hematite concentrations. For low sand concentrations, there is a rapid fall in the dielectric constant with frequency increase at relatively lower frequencies. The dielectric constant of the specimen increases from ~ $2X10^4$ to $2.5X10^7$ for ~ 100 percent hematite concentration (at 0.1 Hz) and with increasing hematite content. The dielectric constant decreases with frequency, with a rapid fall at low frequencies (up to 100 Hz to 1 kHz) and a moderate decrease at higher frequencies. The barriers between differing activation energies between ions and molecules reduce as frequency increases. The crossover frequency between the two slopes ranges between 100 Hz for high sand percentages and 10 kHz for high hematite (or low sand) percentages. The addition of hematite concentrations to the sand percentages enhances the conductor routes (or reduces the distances between sand grains), lowering the dielectric constant. Ionic, electronic, interfacial, and electric dipole polarizations all have a role in determining the dielectric characteristics of samples. All four types of polarization play a role at low frequencies, whereas only electronic and ionic polarization plays a role at high frequencies. Because electronic and ionic polarizations are inherent features of materials and show very minor variation with frequency, a very small variation in the real portion of permittivity concerning frequency is observed in the high-frequency range (Franceschetti and Macdonald 1977; Glover et al. 1994; Huggins 1975; Jonscher 1977; Kurien et al. 2006; Levitskaya and Sternberg 2000; Macdonald1974; Simon and Franke 2000).

Figure 3 depicts the electrical performance of real impedance values as a function of frequency for samples with varied sand percentages (0, 5, 10, 15, 20, 25, 30, 40, 50, 55, 35, 80, 60, 70, 75, 95, 65, 85, 90, and 100 percent). Two slopes are clear of the real impedance values at the curves. There are also two categories of curves. The first group (with a high sand content) displays a practically flat and moderate response to frequency shift. The first group has a relatively high crossover frequency (> 1 kHz) and a low proportion of sand concentration. The second group, on the other hand, has a much lower crossover frequency (1 kHz) and a high sand concentration percentage. For all concentrations, the high-frequency slope of most curves is almost − 1, whereas the lower frequency slope of most curves is nearly zero (except for low sand concentrations). The crossover

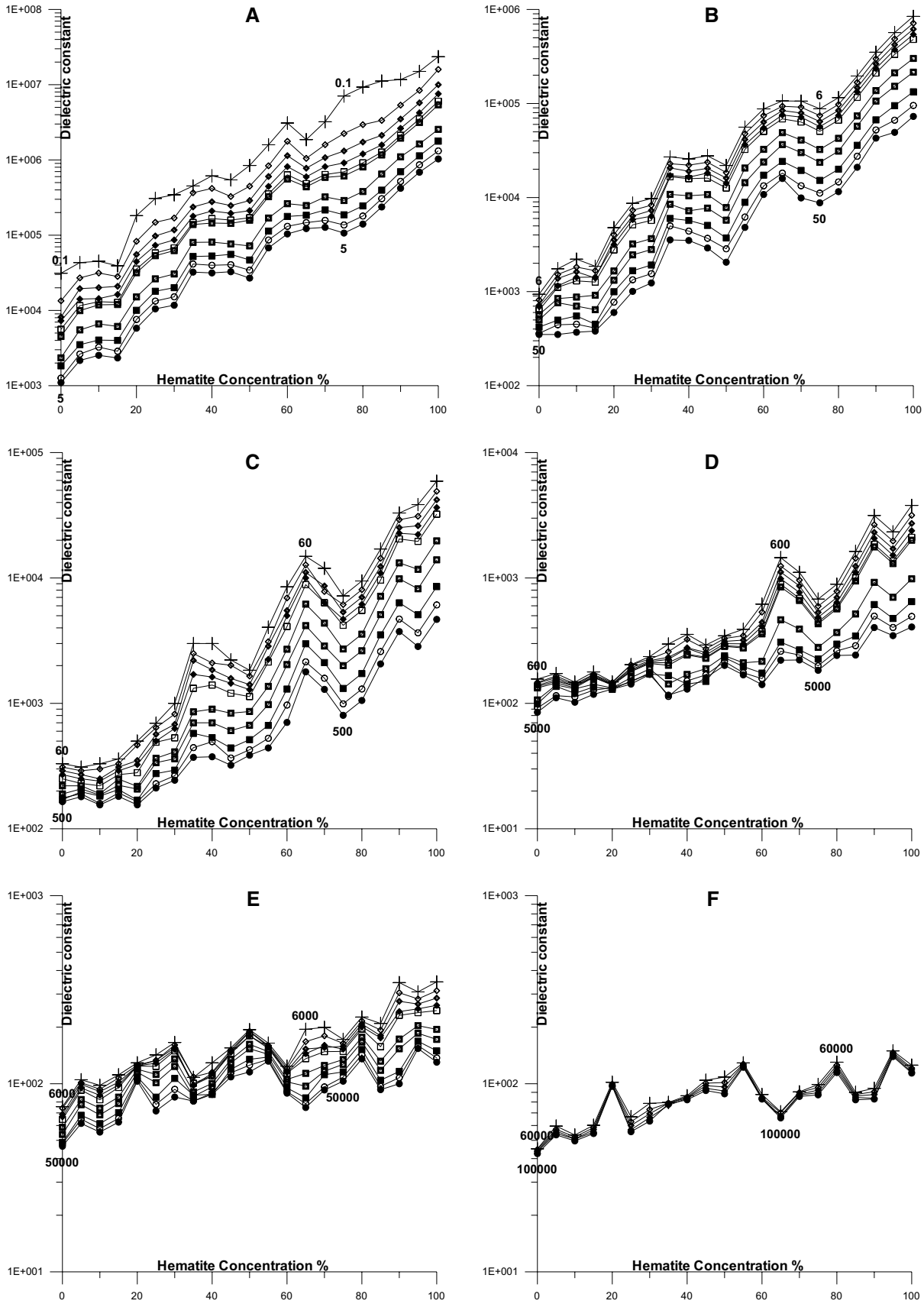
A
Dielectric constant
1E+008
1E+007
1E+006
1E+005
1E+004
1E+003
0.1
0.1
5
5
Hematite Concentration %
0
20
40
60
80
100
B
Dielectric constant
1E+006
1E+005
1E+004
1E+003
1E+002
6
6
50
50
Hematite Concentration %
C
Dielectric constant
1E+005
1E+004
1E+003
1E+002
60
60
500
500
Hematite Concentration %
D
Dielectric constant
1E+004
1E+003
1E+002
1E+001
600
600
5000
5000
Hematite Concentration %
E
Dielectric constant
1E+003
1E+002
1E+001
6000
6000
50000
50000
Hematite Concentration %
F
Dielectric constant
1E+003
1E+002
1E+001
60000
60000
100000
100000
Hematite Concentration %

◂**Fig. 9** Electrical performance of dielectric constant values as a function of hematite concentration percentage for samples with varied frequencies [**A** for 0.1 to 5 Hz; **B** for 6 to 50 Hz; **C** for 60 to 500 Hz; **D** for 600 to 5 kHz; **E** for 6 kHz to 50 kHz; **F** for 60 kHz to 100 kHz].

frequency increases with increasing hematite content; it begins at ~ 100 Hz for high sand concentration and ends at 10 kHz for rising hematite concentration. The crossover frequency almost completely disappears at very high hematite concentrations. There is a fast drop in real impedance with increasing sand concentration at certain frequencies and large sand concentrations. With increasing hematite percentage, the specimen's real impedance increases from ~ $8X10^4$ (for low sand concentration at a particular frequency of 0.1 Hz) to ~ $4X10^7$ (for ~ 100 percent hematite concentration at the same frequency). The real impedance begins steady (with no discernible change) with frequency and then rapidly decreases at higher frequencies. The subsequent reduction in real impedance with an increase at higher frequencies is attributed to the increase in conduction connections at samples. As frequency increases, the barriers between energy levels (between ions and molecules) decrease. The addition of hematite concentrations to the sand percentages enhances the conductor interconnections (or distances between sand grains), decreasing the real impedance values.

Figure 4 depicts the electrical performance of imaginary impedance values as a function of frequency for samples with varied sand percentages (0, 5, 10, 15, 20, 25, 30, 40, 50, 55, 35, 80, 60, 70, 75, 95, 65, 85, 90, and 100 percent). In general, all of the curves follow the same pattern, with a little shift to higher frequencies as sand concentrations expand. The imaginary impedance decreases to a specific limit as frequency increases, then increases to a particular peak frequency, and begins to decrease again associated with a particular slope (the gradient is the same for all samples). The gradient of the initial imaginary impedance decrease, with frequency increase, is of the order of ~ 0.35. The gradient of the second imaginary impedance decrease, with frequency increase, is of the order of ~ 1. The third (final) imaginary impedance rise has a gradient of the order of − 1 as frequency increases. With decreasing sand concentration, the peak of the imaginary impedance changes downward, and its position shifts to higher frequencies. With a reduction in sand concentration percentage, the crossover frequency shifts to higher frequencies. It starts at ~ 100 Hz to represent high sand concentration and finishes at 100 kHz to represent high hematite concentration. The crossover frequency vanishes at very high hematite concentrations (beyond the range of our measurements). With increasing sand concentration, the imaginary impedance values rapidly decrease. As the hematite percentage increases, the specimen's peak imaginary impedance rises from ~ $4X10^3$ (for low sand concentration) to ~ $1.5X10^7$ (for high sand concentration), and the location shifts to higher frequencies. The subsequent decrease in imaginary impedance as hematite concentration increases is related to an increase in conduction connections at samples. The energy levels get nearer as the frequency increases, decreasing the widths between conductor interconnections and decreasing and increasing the imaginary impedance values.

Figure 5 depicts the electrical performance of complex impedance values as a function of frequency for samples with varied sand percentages (0, 5, 10, 15, 20, 25, 30, 40, 50, 55, 35, 80, 60, 70, 75, 95, 65, 85, 90, and 100 percent). All of the curves, in general, follow the same pattern (two attached semicircles). The volume of the complex impedance semicircles (relative to each other), and the peak frequency (or crossover frequency) between the two semicircles, changes from one case to another. The bulk impedance semicircle (at high frequency) and the interface or electrode impedance semicircle (at low frequency) are the two semicircles. As sand concentrations reduce, the peak frequency (or crossover frequency) shifts to higher frequency values, and the overall values of the complex impedance decrease. For large sand concentrations, the complex impedance begins as a simple semicircle (the bulk semicircle). With hematite additions to sand (sand decreases), another connected portion of the semicircle (at low frequencies) begins to develop (the interface semicircle) and grows in diameter with further additions. More hematite additions lead to the generation of two semicircles (the second is not complete). The volume of the interface semicircle gets very large in comparison to the volume of the bulk semicircle until the volume of the bulk semicircle becomes very tiny in comparison with the volume of the interface semicircle at very low sand concentrations. To illustrate the form of each collection of curves, researchers must draw the *X*-axis similarly to the *Y*-axis. As can be observed from the complex impedance values, we attempt

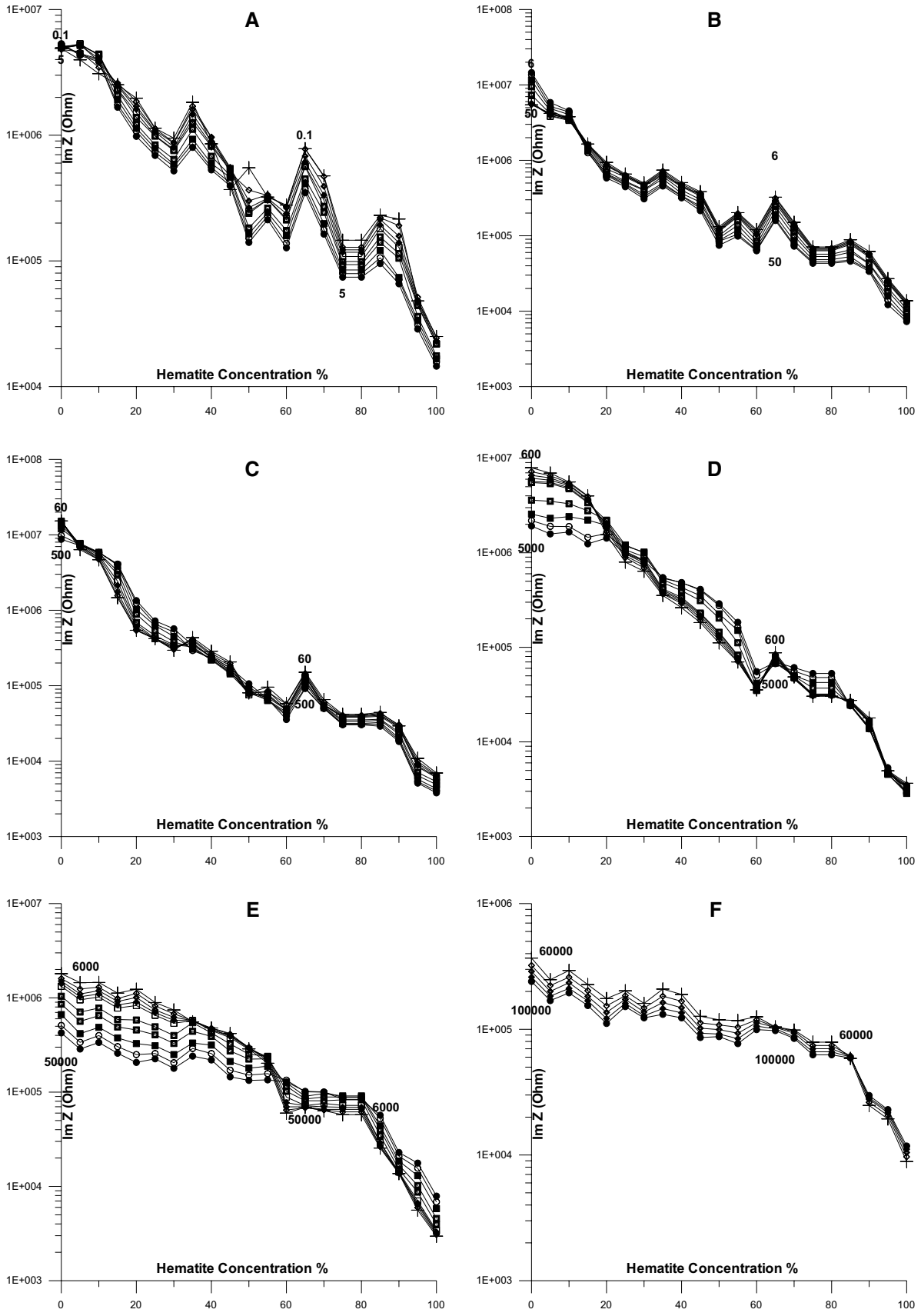
A
B
C
D
E
F
Im Z (Ohm)
Hematite Concentration %
0.1
5
6
50
60
500
600
5000
6000
50000
60000
100000

◂**Fig. 10** Electrical performance of imaginary impedance values as a function of hematite concentration percentage for samples with varied frequencies [**A** for 0.1 to 5 Hz; **B** for 6 to 50 Hz; **C** for 60 to 500 Hz; **D** for 600 to 5 kHz; **E** for 6 kHz to 50 kHz; **F** for 60 kHz to 100 kHz].

to take more than six sets of curves to illustrate the effect of sand reduction (Fig. 5A–F). With increasing sand concentration, the complex impedance's peak shifts downward and to higher frequencies. Moreover, when the proportion of sand concentration increases, the crossover frequency between the two semicircles rises to higher frequencies. The specimen's peak complex impedance reduces as the sand % increases, from ~ $1.5X10^7$ (for low sand concentration) to ~ $4X10^3$ (for high sand concentration). The subsequent rise in conduction connections at specimens is attributed to a decrease in complex impedance as hematite content increases (sand decrease). As the conductor cluster develops, the widths between conductor interconnections shrink.

Figure 6 depicts the electrical performance of phase angle values as a function of frequency for samples with varied sand percentages (0, 5, 10, 15, 20, 25, 30, 40, 50, 55, 35, 80, 60, 70, 75, 95, 65, 85, 90, and 100 percent). All of the curves follow the same pattern, generally. The location of the phase angle peak is not clear (at high or low frequency) within the available frequency range. The phase angle increases with the decrease in sand concentration percentage (at low frequency 0.1 Hz) and it decreases (generally) with the increase in sand concentration percentage (at high frequency > 3 kHz). At ~ 100 Hz, the behavior of the phase angle with sand concentration percentage is reversed. At low frequency (0.1 Hz), the value of the phase angle ranges from 0.1 mrad (for high sand concentration percentage) to 0.6 mrad (for low sand concentration percentage). At high frequency (100 kHz), the value of the phase angle ranges from 0.2 mrad (for low sand concentration percentage) to 5 mrad (for high sand concentration percentage). The subsequent decrease in phase angle with the increase in sand concentration percentage (at a low frequency of 0.1 Hz) is related to a decrease in conduction connections at samples. The subsequent increase in phase angle with the increase in sand concentration percentage (at a high frequency of 100 kHz) is related to an increase in broken linkages at samples. The energy levels get nearer as the frequency increases, decreasing the widths between conductor interconnections and decreasing the phase angle values.

Figure 7 depicts the electrical performance of dielectric loss values as a function of frequency for samples with varied sand percentages (0, 5, 10, 15, 20, 25, 30, 40, 50, 55, 35, 80, 60, 70, 75, 95, 65, 85, 90, and 100%). The degree of actual power dissipation (or losses) in a dielectric medium is measured by the tan δ. If we assume that the resistance of an ideal cable is infinite, the total current will be entirely capacitive and the 90° phase displaced concerning the applied voltage. However, in an actual cable system, losses enable resistive currents to flow, affecting the phase shift of total current concerning voltage. As a result, a loss angle (δ) appears, and its tangent corresponds to tan δ, which is a dimensionless unit. This relationship also shows that as insulation resistance decreases, tan δ increases. The sensitivity is one of the primary benefits of measuring tan δ. One of the primary benefits of measuring tan δ is the increased sensitivity that a lower frequency allows. When $\tan \delta = (2\mathrm{fRC})^{-1}$ is used, where f = frequency, R = resistance, and C = capacitance, it is clear that tan δ is very frequency sensitive. Any rise in the real component of the relative permittivity (capacitance) as frequency increases in the radio-frequency and low microwave bands is nearly invariably attributable to geometrical resonance or other texture-dependent resonance. The imaginary portion of the relative permittivity of lossy materials reduces quicker as frequency increases (dispersion) than it does in non-lossy materials. The imaginary component of the relative permittivity, on the other hand, does not always decrease as frequency increases. It may arise with frequency or generate a Debye loss peak. The dielectric loss angle ($90°–\theta$) is defined as the degree by which the current wave deviates from being 90° out of phase with the voltage. The tan δ or dissipation factor is the tangent of this angle. In terms of frequency and temperature dependence, dielectric loss (tan δ) approximates the imaginary portion of relative permittivity.

Because wavelength decreases with increasing frequency applied to the sample, the decreasing trend of real permittivity concerning frequency is advantageous for surface impedance match. Except for the first few frequencies, the value of actual permittivity has grown with frequency and is likewise increasing with conductor concentration (hematite). It

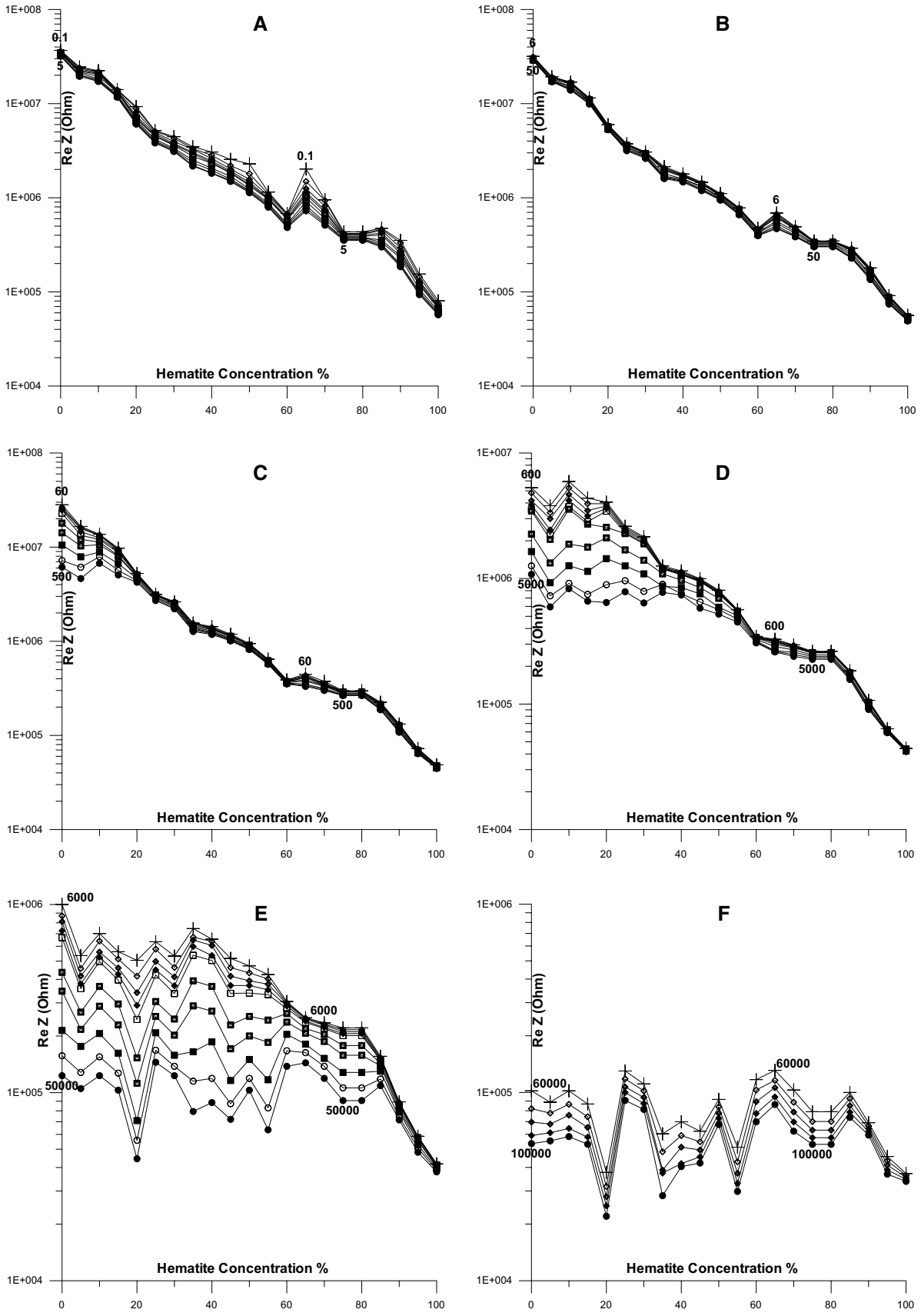
A
B
C
D
E
F
Re Z (Ohm)
Hematite Concentration %
0.1
5
6
50
60
500
600
5000
6000
50000
60000
100000
1E+008
1E+007
1E+006
1E+005
1E+004
0
20
40
60
80
100

◂**Fig. 11** Electrical performance of real impedance values as a function of hematite concentration percentage for samples with varied frequencies [**A** for 0.1 to 5 Hz; **B** for 6 to 50 Hz; **C** for 60 to 500 Hz; **D** for 600 to 5 kHz; **E** for 6 kHz to 50 kHz; **F** for 60 kHz to 100 kHz].

might be related to the fact that as conducting ions increase, more free ions are created, resulting in a rise in free charges. Local electrons or charges are moved in the direction of the applied field, increasing the actual permittivity. In general, most curves exhibit the same behavior (two beaks). Peak values range from 1 to 0.6 at frequencies ranging from 100 Hz to 10 kHz, which vary from case to case.

Figure 8 depicts the electrical performance of conductivity values as a function of hematite concentration percentage for samples with varied frequencies [A) for 0.1 to 5 Hz; B) for 6 to 50 Hz; C) for 60 to 500 Hz; D) for 600 to 5 kHz; E) for 6 kHz to 50 kHz; F) for 60 kHz to 100 kHz]. The overall behavior of the sample groups demonstrates an increase in conductivity with increasing hematite content. There is no difference between curves at low frequencies. There is a minor variation at high frequencies, particularly in the E and F groups. The conductivity increases with increasing hematite content, as shown in Fig. 8A, and the values of the curves fluctuate somewhat. Figure 8B, C illustrates that as hematite content increases, so does conductivity, with no changes in curve values. Figure 8D–F illustrates that there are some significant variations at low frequencies but no fluctuations at high frequencies (Abd El Aziz and Gomaa 2022a, 2022b)

Figure 9 depicts the electrical performance of dielectric constant values as a function of hematite concentration percentage for samples with varied frequencies [A) for 0.1 to 5 Hz; B) for 6 to 50 Hz; C) for 60 to 500 Hz; D) for 600 to 5 kHz; E) for 6 kHz to 50 kHz; F) for 60 kHz to 100 kHz]. The overall behavior of the sample groups shows a rise in dielectric constant with increasing hematite content. The fluctuation of the dielectric constant rises as frequency decreases. For high and low frequencies, the change or variation in the dielectric constant is almost the same (Fig. 9A–E). At high frequencies (Fig. 9F), there are no changes in the values of the curves, and changing the frequency is inefficient

Figure 10 depicts the electrical performance of imaginary impedance values as a function of hematite concentration percentage for samples with varied frequencies [A) for 0.1 to 5 Hz; B) for 6 to 50 Hz; C) for 60 to 500 Hz; D) for 600 to 5 kHz; E) for 6 kHz to 50 kHz; F) for 60 kHz to 100 kHz]. With increased hematite concentration, the sample groups' general behavior demonstrates a reduction in imaginary impedance. Figure 10E, F indicates larger variations, especially at low hematite concentrations

Figure 11 depicts the electrical performance of real impedance values as a function of hematite concentration percentage for samples with varied frequencies [A) for 0.1 to 5 Hz; B) for 6 to 50 Hz; C) for 60 to 500 Hz; D) for 600 to 5 kHz; E) for 6 kHz to 50 kHz; F) for 60 kHz to 100 kHz]. With increased hematite concentration, the sample groups' general behavior demonstrates a reduction in real impedance. Figure 10A–C indicates small variations, at low and high hematite concentrations. Figure 10D–F indicates larger variations, especially at low hematite concentrations.

Figure 12 depicts the electrical performance of tan δ (loss tangent) values as a function of hematite concentration percentage for samples with varied frequencies [A) for 0.1 to 5 Hz; B) for 6 to 50 Hz; C) for 60 to 500 Hz; D) for 600 to 5 kHz; E) for 6 kHz to 50 kHz; F) for 60 kHz to 100 kHz]. With increasing hematite concentration, the general behavior of the sample groups shows no general rise or decrease in tan δ, as shown in Fig. 10A–C. Figure 10D-F indicates a general rise in tan δ when hematite content increases.

Figure 13 depicts the electrical performance of tan δ values as a function of hematite concentration percentage for samples with varied frequencies [A) for 0.1 to 5 Hz; B) for 6 to 50 Hz; C) for 60 to 500 Hz; D) for 600 to 5 kHz; E) for 6 kHz to 50 kHz; F) for 60 kHz to 100 kHz]. The general behavior of the sample groups reveals a little rise in tan δ with increasing hematite content and frequency (Fig. 10A). Figure 10B depicts some tan δ stability as hematite concentration and frequency increase. Figure 10C–F depicts a general reduction in tan δ as hematite concentration and frequency increase

The electrical performance of peak frequency values (the end frequency of the bulk semicircle) for samples is shown in Fig. 14 as a function of hematite concentration percentage. Peak frequency electrical performance increases exponentially as a function of hematite concentration percentage. This suggests that the hematite percentage is an important factor in determining peak frequency values. It also indicates that as the percentage of the conductor in the samples increases, so do the peak frequency values.

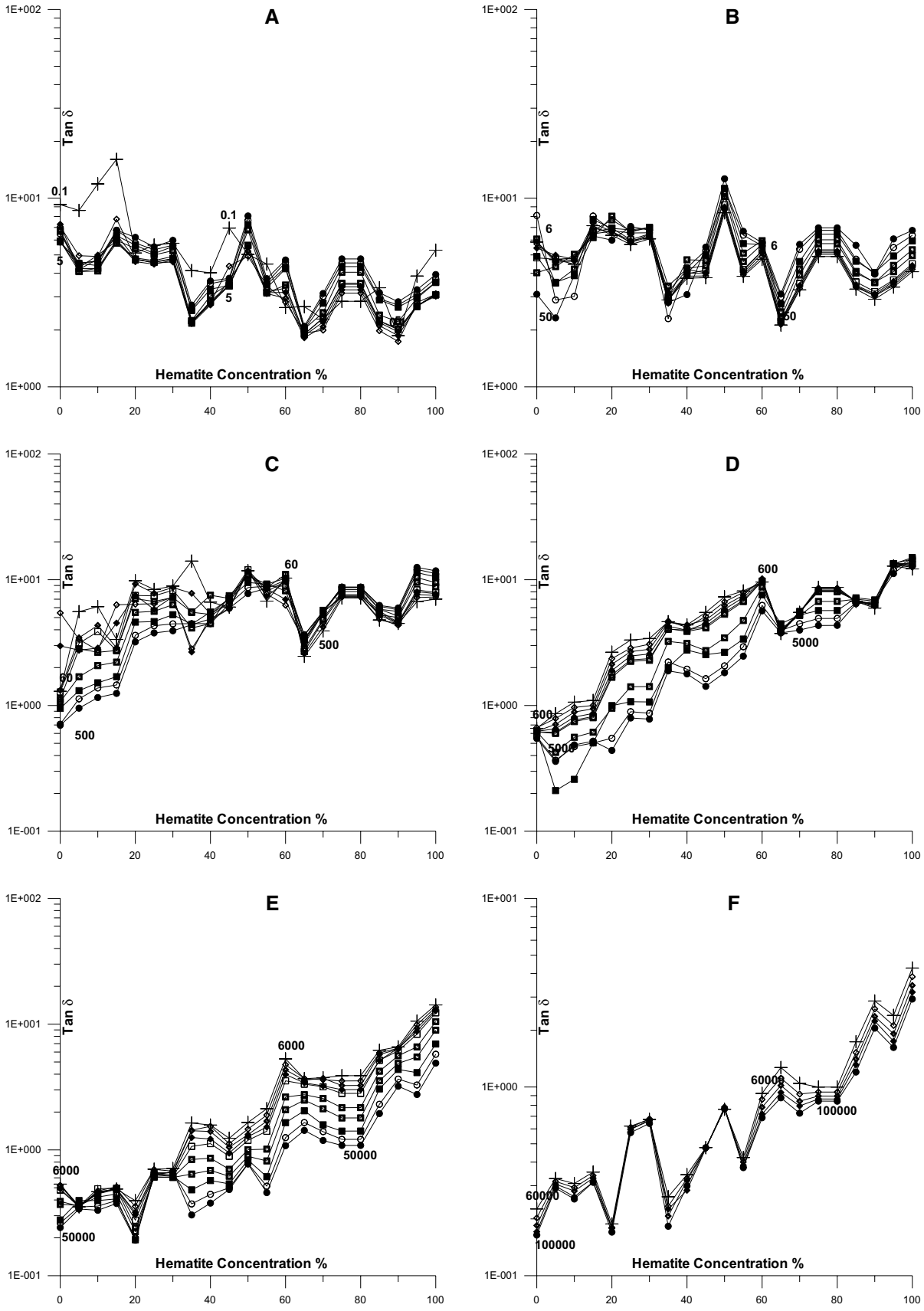
A
B
C
D
E
F
Tan δ
Hematite Concentration %
1E+002
1E+001
1E+000
1E-001
0
20
40
60
80
100
0.1
5
6
50
60
500
600
5000
6000
50000
60000
100000

◂**Fig. 12** Electrical performance of tan δ (loss tangent) values as a function of hematite concentration percentage for samples with varied frequencies [A for 0.1 to 5 Hz; B for 6 to 50 Hz; C for 60 to 500 Hz; D for 600 to 5 kHz; E for 6 kHz to 50 kHz; F for 60 kHz to 100 kHz].

Figure 15 depicts the electrical performance of the actual impedance of the peak frequency values for samples as a function of hematite concentration percentage. The real impedance of peak frequency performance drops rapidly as a function of hematite concentration percentage. This implies that as the percentage of the conductor in the samples grows, the true impedance of the peak frequency values decreases.

The electrical performance of the imaginary impedance of the peak frequency values for samples as a function of hematite concentration percentage is shown in Fig. 16. The peak frequency performance's imaginary impedance decreases significantly as a function of hematite concentration percentage. This means that as the fraction of conductor in the samples increases, so does the imaginary impedance of the peak frequency values.

The electrical performance of the dielectric constant of the peak frequency values for samples as a function of hematite concentration percentage is shown in Fig. 17. The peak frequency performance's dielectric constant fluctuates significantly (maybe with a general decrease) as a function of hematite concentration percentage. This indicates that the dielectric constant of the peak frequency values increases as the proportion of conductors in the samples increases.

The electrical performance of the dielectric loss of the peak frequency values for samples as a function of hematite concentration percentage is shown in Fig. 18. The peak frequency performance's dielectric loss fluctuates greatly (with no general decrease or increase) as a function of hematite concentration percentage. This indicates that the dielectric loss of the peak frequency values increases as the proportion of conductors in the samples increases.

The electrical performance of the conductivity of the peak frequency values for samples as a function of hematite concentration percentage is shown in Fig. 19. The peak frequency performance's conductivity increases greatly as a function of hematite concentration percentage. This indicates that the conductivity of the peak frequency values increases as the proportion of conductors in the samples increases.

The electrical performance of the tan δ of the peak frequency values for samples as a function of hematite concentration percentage is shown in Fig. 20. The peak frequency performance's tan δ increases slightly as a function of hematite concentration percentage.

The electrical performance of the phase (Rad) of the peak frequency values for samples as a function of hematite concentration percentage is shown in Fig. 21. The peak frequency performance phase decreases slightly as a function of hematite concentration percentage. This indicates that the phase (Rad) of the peak frequency values increases as the proportion of conductors in the samples increases.

Conclusion

The electrical properties of composites are influenced by the amounts of their constituents as well as their texture. This study looked into the relationships between the ore's nature, its mineral group, and their relationship to electrical properties (homogeneity and concentration of constituents). Electrical parameters were examined at frequencies ranging from 0.1 to 10^5 Hz (dry, 21 °C). The dielectric constant and conductivity of the samples rise as the hematite content increases. The frequency dependence of conductivity is consistent with Jonscher's law (increase in charge carriers and mobility of charges). As the concentration of hematite increases, so do the permittivity and the number of component clusters. The rise in loss factor with concentration is caused by interface or space charge polarization and changes in conductivity values (there are many relaxation times). The complex impedance response was presented as a semicircle attached to an arc. In general, as hematite concentration increases, the semicircle shrinks (or disappears) and the diffusion or Warburg impedance (straight line or arc) takes over. A high-frequency semicircle is thought to depict ion exchange at grain surfaces, whereas a low-frequency arc is thought to represent diffusion and transport of generated charge carriers. This study is valuable for exploration methods and modeling of the electrical properties of rocks.

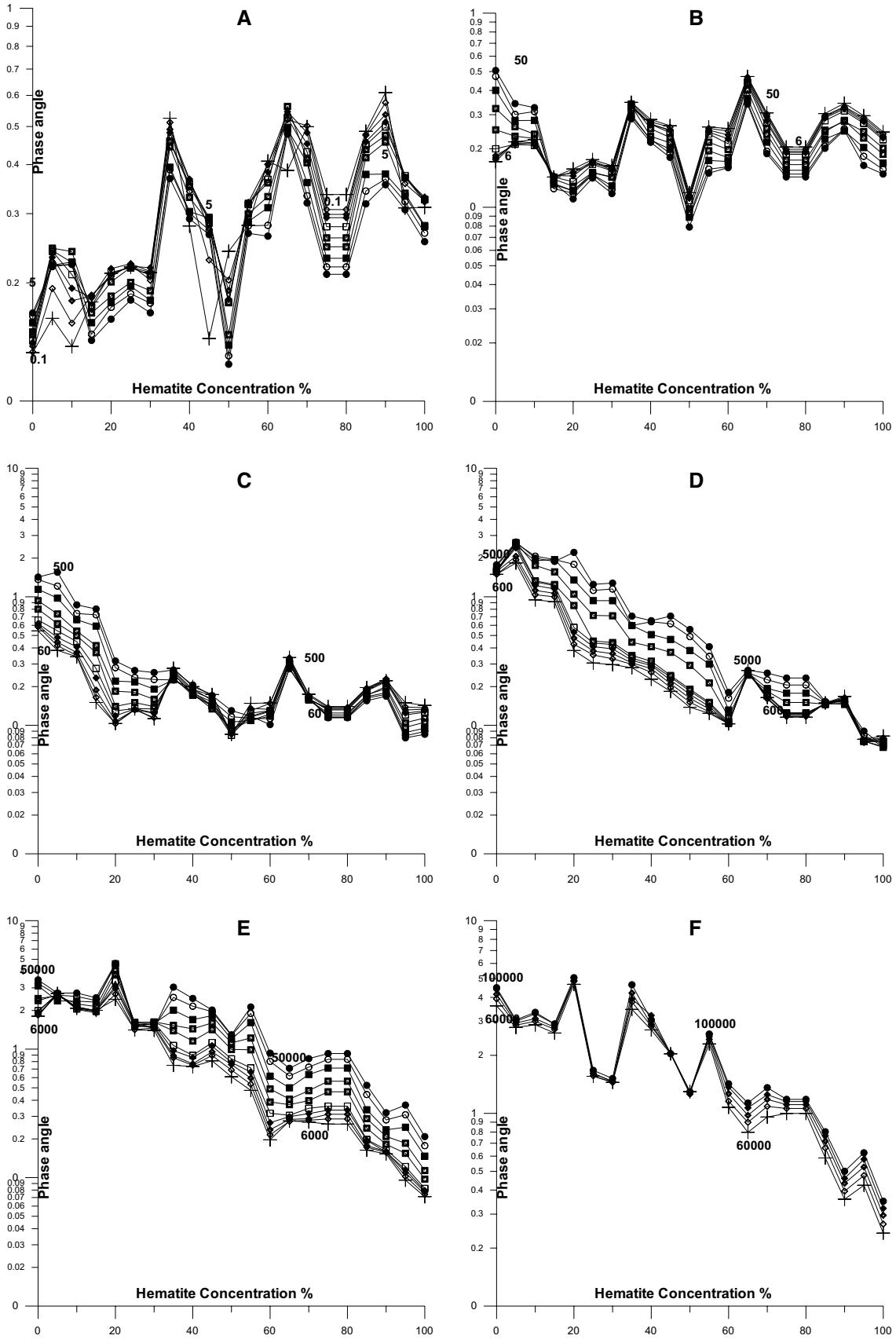
A
Phase angle
Hematite Concentration %
0.1
5
5
0.1
5
B
Phase angle
Hematite Concentration %
50
6
50
6
C
Phase angle
Hematite Concentration %
500
60
500
60
D
Phase angle
Hematite Concentration %
5000
600
5000
600
E
Phase angle
Hematite Concentration %
50000
6000
50000
6000
F
Phase angle
Hematite Concentration %
100000
60000
100000
60000

◂**Fig. 13** Electrical performance of phase angle values as a function of hematite concentration percentage for samples with varied frequencies [**A** for 0.1 to 5 Hz; **B** for 6 to 50 Hz; **C** for 60 to 500 Hz; **D** for 600 to 5 kHz; **E** for 6 kHz to 50 kHz; **F** for 60 kHz to 100 kHz].

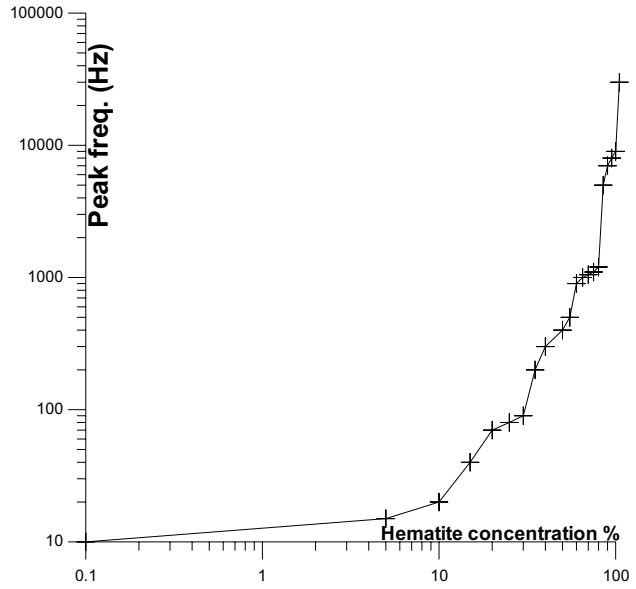

Fig. 14 Electrical performance of peak frequency values (end frequency of the bulk semicircle) as a function of hematite concentration percentage for samples.

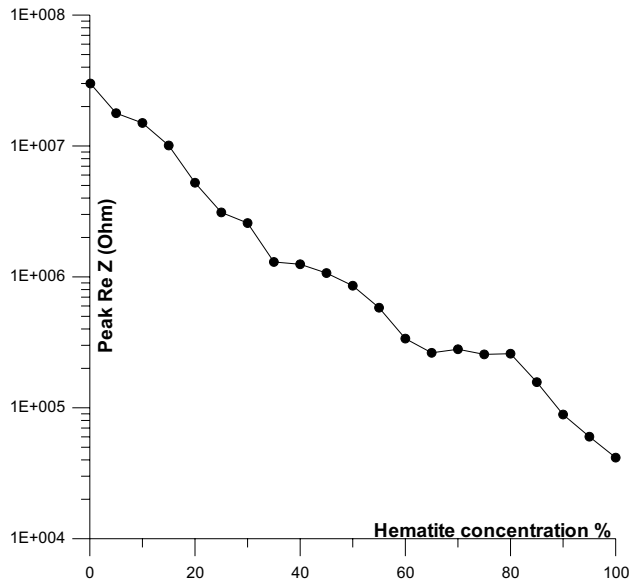

Fig. 15 Electrical performance of real impedance of the peak frequency values (end frequency of the bulk semicircle) as a function of hematite concentration percentage for samples.

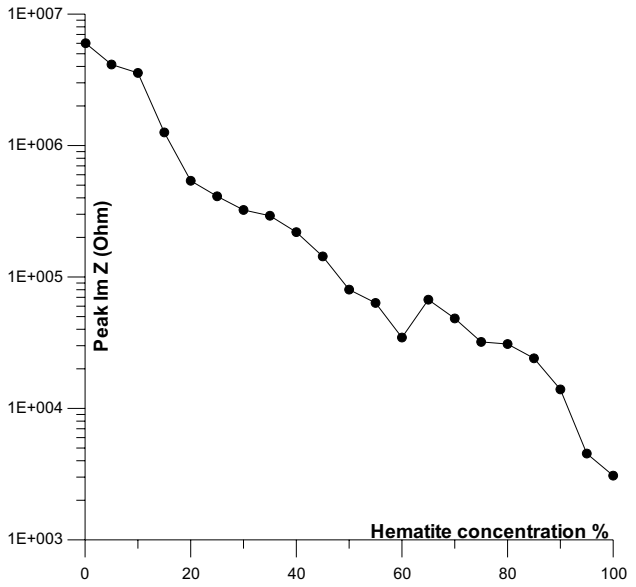

Fig. 16 Electrical performance of imaginary impedance of the peak frequency values (end frequency of the bulk semicircle) as a function of hematite concentration percentage for samples.

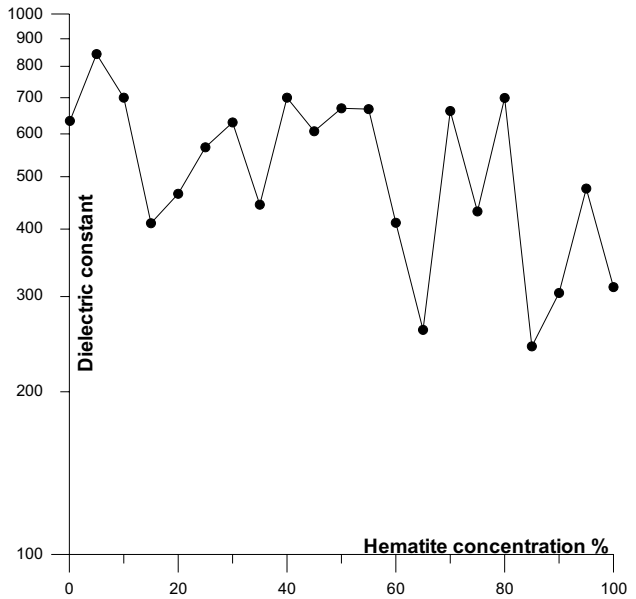

Fig. 17 Electrical performance of the dielectric constant of the peak frequency values (end frequency of the bulk semicircle) as a function of the hematite concentration percentage for samples.

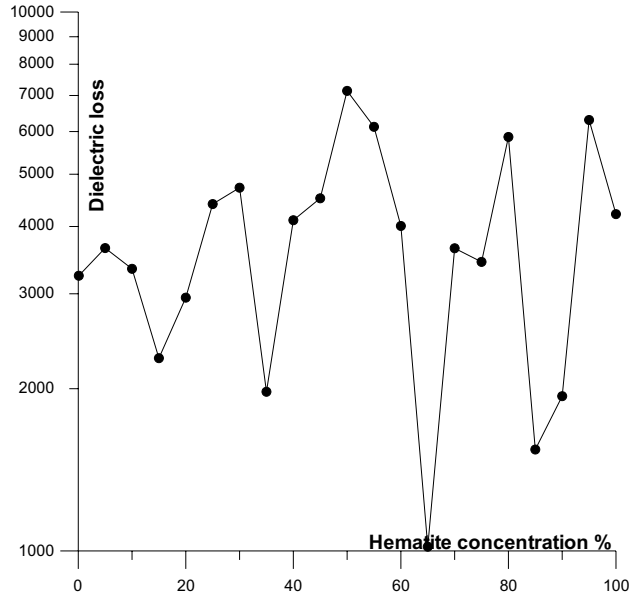

Fig. 18 Electrical performance of dielectric loss of the peak frequency values (end frequency of the bulk semicircle) as a function of hematite concentration percentage for samples.

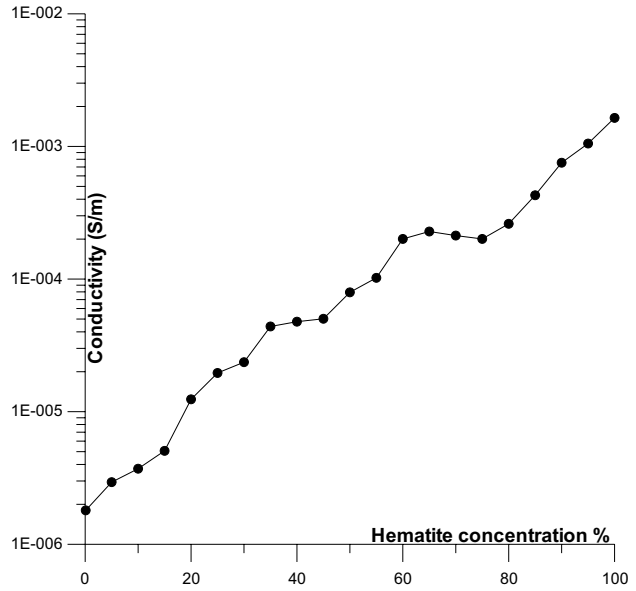

Fig. 19 Electrical performance of the conductivity of the peak frequency values (end frequency of the bulk semicircle) as a function of hematite concentration percentage for samples.

Acknowledgements I would like to send a great thanks to the National Research Centre.

Author contributions ME shared and contributed in planning, conducting, and reporting of the work described in this article. MMG shared and contributed in planning, conducting, and reporting of the work described in this article. MR shared and contributed in planning, conducting, and reporting of the work described in this article.

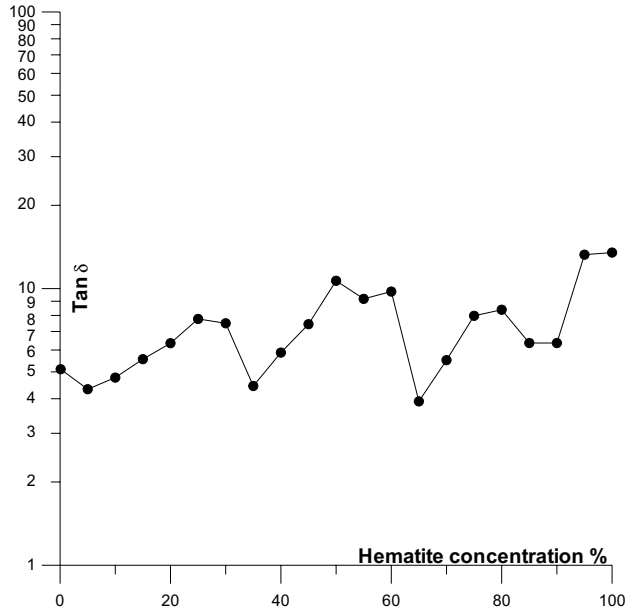

Fig. 20 Electrical performance of tan δ of the peak frequency values (end frequency of the bulk semicircle) as a function of hematite concentration percentage for samples.

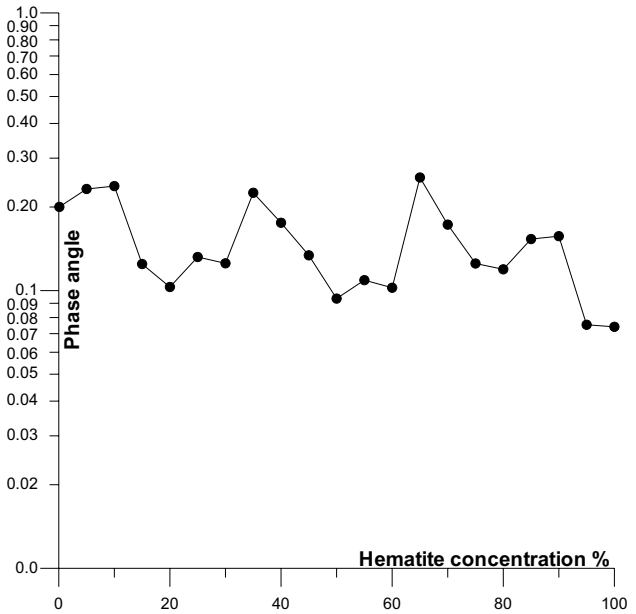

Fig. 21 Electrical performance of phase (Rad) of the peak frequency values (end frequency of the bulk semicircle) as a function of hematite concentration percentage for samples.

Funding Open access funding provided by The Science, Technology & Innovation Funding Authority (STDF) in cooperation with The Egyptian Knowledge Bank (EKB). No funding was received.

Data availability All data generated or analyzed during this study are included in this published article.

Availability of data and materials The data that support the findings of this study are available within the article.

Declarations

Competing interests The authors declare that there are no competing interests to disclose in relation to the work described.

References

Abd El Aziz EA, Gomaa MM (2022a) Petrophysical analysis of well logs and core samples for reservoir evaluation: a case study of southern Issaran Field Gulf of Suez Province, Egypt. Environ Earth Sci. https://doi.org/10.1007/s12665-022-10420-x

Abou E-A, Gomaa MM (2013) Electrical properties and geochemistry of carbonate rocks from the Qasr El-Sagha formation El-Faiyum, Egypt. Geophys Prospect 61:630–644

Attia, M. I., Topography, geology and iron-ore deposits of the district east of Aswan. Geol. Surv., Cairo, Egypt, p. 262, 1955.

Aziz EA, Gomaa MM (2022b) Electrical properties of sedimentary microfacies and depositional environment deduced from core analysis of the syn-rift sediments, northwestern shore of Gulf of Suez Egypt. J Pet Explor Prod Technol 12:2915–2936. https://doi.org/10.1007/s13202-022-01484-3

Capozzoli L, Giampaolo V, De Martino G, Gomaa M, Rizzo E (2022) Geoelectrical measurements to monitor a hydrocarbon leakage in the aquifer: simulation experiment in the lab. Geosciences 12(10):360–374. https://doi.org/10.3390/geosciences12100360

Chelidze T, Gueguen Y (1999) Electrical spectroscopy of porous rocks: a review-I. Theor Models Geophys J Int 137:1–15

Chelidze T, Gueguen Y, Ruffet C (1999) Electrical spectroscopy of porous rocks: a review-II. Experimental results and interpretation. Geophys J Int 137:16–34

Chew WC, Sen PN (1982) Dielectric enhancement due to electrochemical double layer: thin double layer approximation. J Chem Phys 77(9):4683–4693

Chirita M, Grozescu I (2009) Fe_2O_3–Nanoparticles, physical properties and their photochemical and photoelectrochemical applications. Chem Bull 54(68):1–8

De Lima OAL (1995) Water saturation and permeability from resistivity, dielectric, and porosity Logs. Geophysics 60(6):1751–1764

De Lima OAL, Sharma MM (1992) A generalized Maxwell-Wagner theory for membrane polarization in shaly sands. Geophysics 57:789–799

Dias CA (1972) Analytical model for a polarizable medium at radio and lower frequencies. J Geophys Res 77(25):9445–4956

Dukhin SS, Shilov VN (1974) Dielectric phenomena and the double layer in disperse systems and polyelectrolytes. John Wiley and Sons, New York

Franceschetti DR, Macdonald JR (1977) electrode kinetics, equivalent circuits, and system characterization: small-signal conditions. J Electroanal Chem 82:271–301

Gason SJ, Boger DV, Dunstan DE (1999) Rheo-optic geological evidences on the paleogeography of the nubian sandstone. Langmuir 1999(15):7446–7453

Glover PWJ, Meredith PG, Sammonds PR, Murrel SAF (1994) Ionic surface electrical conductivity in sandstone. J Geophys Res 99(B11):21635–21650

Gomaa MM (2006) Interpretation of electrical properties for humid and saturated hematitic sandstone sample, presented at the 68th conference and exhibition incorporating SPE Europe: European association of geoscientists and engineers (EAGE), Oral H021. Session "Gravity, Magnetics, Mining and Geothermal", Opportunities in mature areas 4:12–15. Vienna, Austria, pp. 2182–2186

Gomaa MM (2008) Relation between electric properties and water saturation for hematitic sandstone with frequency. Ann Geophys 51(5/6):801–811

Gomaa MM (2009) Saturation effect on Electrical properties of hematitic sandstone in the audio frequency range using non-polarizing electrodes. Geophys Prospect 57:1091–1100

Gomaa MM (2013) Forward and inverse modeling of the electrical properties of magnetite intruded by magma Egypt. Geophys J Int 194(3):1527–1540

Gomaa MM (2022) Grain size effect on electrical properties of dry friable sand. Eur Phys J Spec Top. https://doi.org/10.1140/epjs/s11734-022-00667-7

Gomaa MM, Abou E-A (2017) Electrical, mineralogical, and geochemical properties of Um Gheig and Um Bogma formations. Egypt, Carbonates and Evaporites, pp 1–14

Gomaa MM, Alikaj P (2009) Effect of electrode contact impedance on a. c. electrical properties of wet hematite sample. Mar Geophys Res 30(4):265–276

Gomaa MM, Elsayed RM (2009) Thermal effect of magma intrusion on electrical properties of magnetic rocks from hamamat sediments NE Desert, Egypt. Geophys Prospect 57(1):141–149

Gomaa MM, Kassab M (2016) Pseudo random renormalization group forward and inverse modeling of the electrical properties of some carbonate rocks. J Appl Geophys 135:144–154

Gomaa MM, Kassab M (2017) Forward and inverse modelling of electrical properties of some sandstone rocks using renormalization group method. Near Surf Geophys 15(5):487–498

Gomaa MM, Kassab M, El-Sayed NA (2015) Study of petrographical and electrical properties of some Jurassic carbonate rocks, north Sinai, Egypt, Egyptian. J Petroleum 24(3):343–352

Gomaa MM, Shaltout A, Boshta M (2009) Electrical properties and mineralogical investigation of Egyptian iron ore deposits. Mater Chem Phys 114(1):313–318

Gomaa MM, Metwally H, Melegy A (2018) Effect of concentration of salts on electrical properties of sediments, Lake Quaroun, Fayium, Egypt. Carbonates Evaporites 34(3):721–729

Gomaa MM, Hussain SA, El-Diwany EA, Bayoumi AE, Ghobashy MM (2000) Modeling of A. C. electrical properties of humid sand and the effect of water content, Society of Exploration Geophysicists, (SEG). International exposition and 70th annual meeting, Calgary, Alberta, Canada, 19 (1):1850–1853

Gomaa MM, Hussain SA, El-Diwany EA, Bayoumi AE, Ghobashy M. (1999) Pseudo-random network modelling of electrical properties of natural hematitic sandstone. 61st Technical programme meeting: European association of geoscientists and engineers (EAGE), Oral 2022, Session "Rock Physics II", 7–11, Helsinki Fair Centre, Finland

Huggins RA. Diffusion in Solids: recent Developments. Nowick AS, Burton Ie J. (Eds.), (Academic Press, New York, 1975)

Jonscher AK (1977) Review article the universal dielectric response. Nature 267:673–679
Jonscher AK (1999) Dielectric relaxation in solids. J Phys D Appl Phys 32:R57–R70
Kassab M, Gomaa MM, Lala A (2017) Relationships between electrical properties and petrography of El-Maghara sandstone formations Egypt. NRIAG J Astronom Geophys 6:162–173
Knight R (1983) The use of complex plane plots in studying the electrical response of rocks. J Geomag Geoelectr 137:767–776
Knight R, Abad A (1995) Rock/water interaction in dielectric properties: experiments with hydrophobic sandstones. Geophysics 60(2):431–436
Knight RJ, Endres AL (1990) A new concept in modeling the dielectric response of sandstones: defining a wetted rock and bulk water system. Geophysics 55:586–594
Knight RJ, Nur A (1987) The dielectric constant of sandstones, 50 kHz to 4 MHz. Geophysics 52:644–654
Kurien S, Mathew J, Sebastian S, Potty SN, George KC (2006) Dielectric behavior and ac electrical conductivity of nanocrystalline nickel aluminate. Mater Chem Phys 98:470–476
Levitskaya TM, Sternberg BK (2000) Application of lumped-circuit method to studying soils at frequencies from 1 kHz to 1 GHz. Radio Sci 35(2):371–383
Lima De OAL, Sharma MM (1991) Water conductivity and saturation effects on the dielectric response of shaly sands. 32nd Ann Log Symp Trans Soc Prof Well Log Analysts. Paper G
Macdonald JR (1974) Some AC response results for solids with recombining space charge. J Phys C Solid State Phys 7:L327–L331
Marshall DJ, Madden TR (1959) Induced polarization, a study of its causes. Geophysics 24(4):790–816
Nakhla FM, Shehata MRN (1967) Contributions to the mineralogy and geochemistry of some iron-ore deposits in Egypt (UAR). Miner Depos 2:357–371
Olhoeft GR (1985) Low frequency electrical properties. Geophysics 137:2492–2503
Sen PN (1981) Dielectric anomaly in inhomogeneous materials with application to sedimentary rocks. Appl Phys Lett 39(8):667–668
Sen PN (1984) Grain shape effects on dielectric and electrical properties of rocks. Geophysics 49:586–587
Sen PN (1989) Unified models of conductivity and membrane potential of porous media. Phys Rev B 137:9508–9517
Shaltout AA, Gomaa MM, Wahbe M (2012) Utilization of standardless analysis algorithms using WDXRF and XRD for Egyptian Iron Ores identification. X-Ray Spectrom 41:355–362
Shukri NM, Ayouty A (1959) The mineralogy of the Nubian sandstone in Aswan. Bull Inst Desert Egypt 3(2):65–88
Simon U, Franke ME (2000) Electrical properties of nanoscaled host/guest-compounds. Microporous Mesoporous Mater 41:1–36
Taylor SR, Ahrens LH (1960) Spectrochemical analysis in "Methods in Geochemistry". Smales AA Wager LR, 81–110
Vinegar HJ, Waxman MH (1984) Induced polarization of shaly sands. Geophysics 49:1267–1287